American Mineralogist, Volume 67, pages 521–533, 1982

Elemental mapping of minerals by electron microprobe

W. JANSEN

Perkin-Elmer/Physical Electronics Division
1161-C San Antonio Road
Mountain View, California 94043

AND M. SLAUGHTER

Department of Chemistry and Geochemistry
Colorado School of Mines
Golden, Colorado 80401

Abstract

The electron microprobe produces two-dimensional images of elemental distributions by displaying X-ray photon-caused pulses on a cathode ray tube as the electron beam scans the sample. The usefulness of the microprobe in mineralogy, diminished by this inaccurate qualitative elemental recording method, increases significantly with quantification of two-dimensionally collected X-ray intensities. A simple interrupt circuit added to the microprobe's electron beam scanner defines the raster rate for a data collection computer. The computer, monitoring the X-ray spectrometers through counters, collects X-ray intensities at peak and background spectrometer positions from a rectangular grid of 2,000 points from single or multiple rasters. Standards, scanned in the same manner as analytes, give a grid of X-ray intensities defining a least-squares fitted surface to compensate for areal defocusing of the spectrometers, and to quantify sample composition. Smoothing eliminates spurious intensities caused by counting statistics and sample surface irregularities. Measurement of up to eight elements per sample permits first-principles matrix corrections with mass-absorption coefficients, *etc*. The computer groups the 2000 data points into compositional families to make matrix correction calculations practical. The computer plots contour maps of elemental distributions or ratios with or without matrix correction and quantification. Compositional mapping enhances the probe's areal sensitivity and utility.

Introduction

The electron microprobe determines *in-situ* elemental composition and distribution for minerals on a microscopic scale, presenting quantitative X-ray information about elemental concentrations on the surface of polished specimens. An electron beam scans the surface of the sample, three different ways: spot, line, or rectangular area. The spot and line modes produce quantifiable elemental concentrations but recording techniques usually limit the presentation of areal elemental distribution to dots on a photograph.

The inadequacy of the standard microprobe as a quantitative areal elemental analyser is illustrated through an example. Figure 1 shows a typical elemental distribution X-ray dot picture. Each dot represents a detected X-ray photon characteristic of calcium. The relative density of the dots shows the distribution of the calcium concentration in the large triangular zoned plagioclase crystal located in the lower half of Figure 2. Although the dots in Figure 1 give a reasonable outline for the crystal, the plagioclase zoning is barely discernible. Superimposed dots are not distinguished so that small areas of high calcium concentration are not identified. The low density of the dots, even within the area covered by the crystal, makes the resulting dot image statistically unreliable. Increasing the number of dots by slowing the frame rate or by increasing the electron beam current exacerbates the problem of superimposed dots. The dot photographs give inaccurate elemental concentrations because the need to produce enough dots to be statistically satisfactory conflicts with the necessity to reduce the number of dots to avoid dot overlap.

Should quantitative areal analysis be possible,

0003–004X/82/0506–0521$02.00

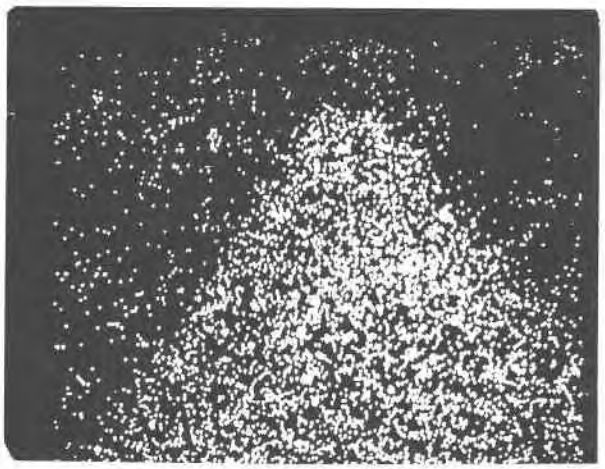

Fig. 1. Beam scanner dot photograph of calcium distribution in a zoned plagioclase feldspar.

the increased sensitivity, ease of interpretation, and quantitative results would make such a technique useful in a variety of mineralogical and petrological applications. Also, contour maps of elemental concentration ratios would indicate important mineralogical zoning and microchemistry of geological samples.

The purpose of this research was to investigate the problems and requirements of areally analyzing rock and mineral samples with the electron microprobe and the collection and modification of X-ray intensities to give quantitative elemental concentrations in rock or mineral specimens.

Several previous attempts have been made to quantify areal elemental concentrations with the electron microprobe. The collection of location-specific X-ray intensities has been introduced but no methods to convert X-ray intensities to elemental concentrations resulted. Research emphasis has been on the improvement of the display on the beamscanner oscilloscope. Birks (1971) showed how X-ray intensities collected from a grid of points using a multi-channel analyzer produce a perspective dot topograph on an oscilloscope when the vertical displacement of each dot is determined by the intensity of the X-rays at the corresponding grid position of each counting channel. A related method displays iso-intensity contours drawn manually on a grid of X-ray intensities printed by a teletype from multichannel analyzer data. Combining line and raster modes, Heinrich (1964) produced deflection and intensity modulated lines, starting at obliquely displaced points, suggesting a topographic image. Tomura *et al.* (1968) introduced a technique called "content mapping" which grouped counts from a 50 × 50 grid of points into intensity ranges. A pulser used the ranges to modulate the brightness of a cathode ray tube on a logarithmic scale. Other methods, usually applying photographic techniques, produce dot photographs to give multiple exposure and color-coded images to show elemental distribution (Ingersoll, 1969; Hitchings, 1976).

None of these older methods relate sample X-ray intensities to standard X-ray intensities; none acount for X-ray fluorescence, absorption, or atomic number effects; none consider spectrometer defocusing at image edges nor allow subtraction of background X-ray intensities.

This paper describes the conception, development, and examples of contoured areal electron beam microanalysis.

Experimental

Instrumentation

We used a Philips PH 4500 electron microprobe microanalyzer referred to subsequently as the EM. The EM has four focusing curved crystal X-ray spectrometers and a beam scanner to record X-ray spectra. All functions of the EM are standard and non-automated. There were no modifications to the EM except to add a small electronic circuit to the beam scanner to send some of its timing pulses to a computer.

To collect X-ray data and to perform the other tasks necessary for areal mapping, we used a Hon-

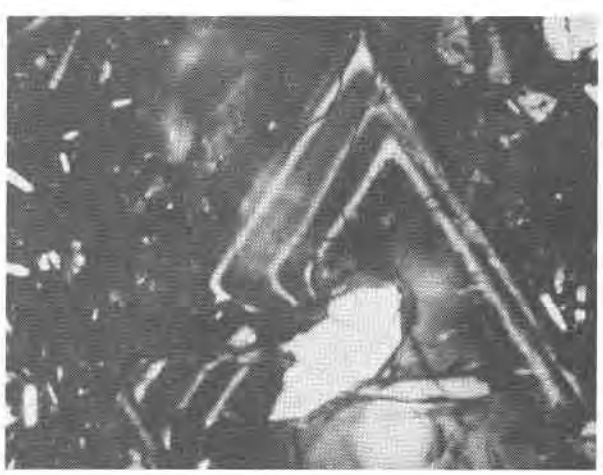

Fig. 2. Photomicrograph of the plagioclase crystal of Figure 1, showing zones. Crossed Nicols.

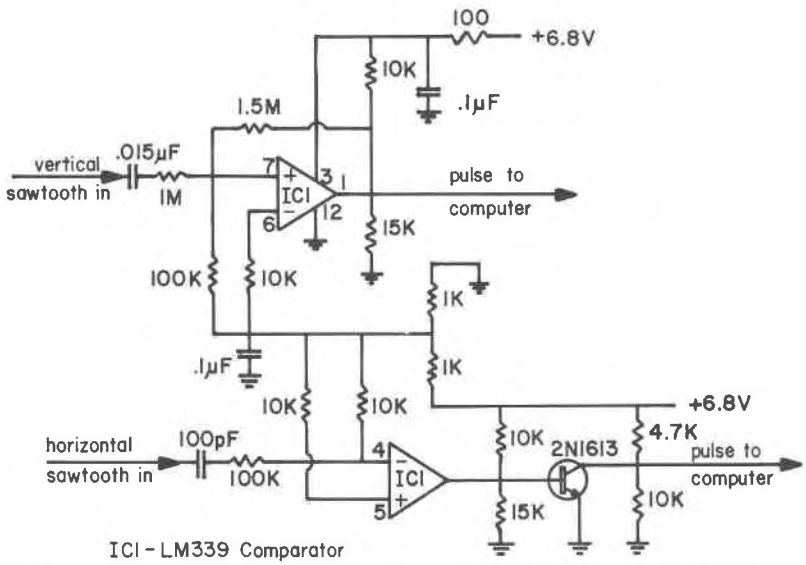

Fig. 3. Electronic circuit to transmit timing signals from an EM beam scanner to a computer.

eywell H316 minicomputer, designed for real-time on-line data aquisition. The computer, with a small plotter attached, accumulated X-ray intensities using four 24-bit binary counters, one for each spectrometer.

The modification to the EM to permit it to communicate its status to the computer is shown in Figure 3. This small circuit, or a variation of it, will allow any older EM to do areal mapping. Newer EM's provide necessary signals as standard options. To produce the pulses sent to the computer, the circuit of Figure 3 differentiates the time-based sawtooth from the vertical (Y) deflection generator. When the differential becomes negative at the end of the vertical sweep, a pulse goes to an interrupt line of the computer. The circuit operates the same way on the horizontal (X) time-based sawtooth, except that it sends a pulse on another interrupt line to the computer. The horizontal sweep pulse tells the computer that a new line has begun. By comparing the number of horizontal lines since the last vertical return sweep to the number of horizontal lines per image, the computer determines the Y position of the microanalyzer electron beam. Using the elapsed time since the last horizontal retrace, the computer determines the X position of the electron beam.

Methods

The experimental procedures and problems can be summarized as follows. Data collection requires that an EM spectrometer be positioned on an elemental X-ray line or its background. The EM must raster the beam while sending beam position information to the computer. The computer, through the counters, must collect data on the grid over the rastered area. The computer has to accumulate the counts in an array, one number per element (or spectrometer) for each square of the grid.

The X-ray intensities collected thus are neither qualitatively correct nor acceptable for mapping. Statistical errors of the X-ray photon counts and the surface topography of the sample introduce spurious apparent concentration highs and lows from a chemically uniform sample, requiring more or less smoothing to help remove small-scale, spurious concentration highs and lows. At magnifications of 500× or below, spectrometers become defocused at extremes of the beam raster, generating a curved intensity surface over the scanned area. To make intensities a function of element concentration, the curved intensity surface must be corrected or normalized to a plane of uniform relative intensity over the whole area. Elemental concentrations from the areally collected X-ray intensities require matrix and other corrections to derive concentration functions. Unfortunately, it is impractical to correct the intensities from each grid square individually because the correction computation requires about 10 seconds for each square. Practicality demands a correction strategy to shorten calculations to a few minutes. Finally, the ability to make areal concentration contour maps also allows presentation of element ratio maps which for many problems

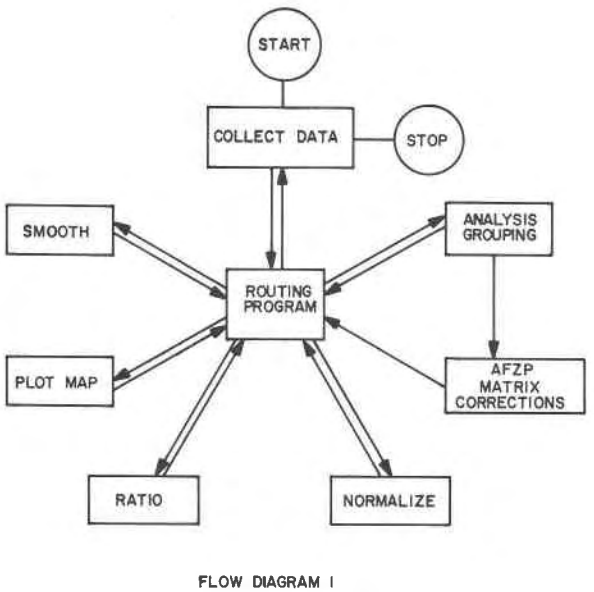

Fig. 4. Calculation flow summary of data collection and data processing to produce qualitative or quantitative concentration contour maps.

should be the most useful data presentation method.

The following sections detail the problems and procedures to obtain elemental concentration maps. Figure 4 summarizes the calculation flow.

X-ray intensity collection

To collect areal X-ray intensities the electron beam must move with respect to the sample. This relative motion can be effected in two ways, electronically or mechanically. Mechanical beam tracking collects X-ray data while the sample is moved under a stationary electron beam. Electronic beam tracking collects X-ray data as the electron beam rasters over the surface of a stationary sample. In the electronic mode the beamscanner controls the beam motion, thereby forcing a particular data collection rate. We investigated both methods but present only the electronic tracking method. Each method has advantages.

To collect data using electronic beam tracking, one must coordinate computer and beam scanner action. The electron beam can be timed as it moves over the stationary sample under control of the beam scanner. Because the beam sweep rates are very stable, timing of the beam is an accurate method of locating beam position. Accurate location of the beam requires determining precisely the point at which timing begins in relation to the position of the electron beam. The horizontal return sweep initiates the time defining the X position of the electron beam and causes an interrupt pulse to the computer. The vertical return sweep defines the Y position of the electron beam and also generates an interrupt pulse to the computer.

After the horizontal interrupt, the X-ray photon counters must be read consecutively causing the sample squares for each element to be offset slightly with respect to each other. The greatest relative shift is less than a width of a line on a contour map and can be ignored. The computer sums intensity data from eleven horizontal sweeps to generate one row of matrix data, giving a representative sampling of the total square area on the sample surface. A 50 column by 40 row data matrix was chosen for scanning after experimenting with various matrix sizes ranging from 30 × 24 to 100 × 80. A smaller number of squares results in insufficient resolution on the contour map. A larger number of squares reduces the counting time per square necessitating much longer data accumulation times.

On the oscilloscope the rectangular image width-to-height ratio is five to four, the same as the data matrix dimensions. At a frame rate of one per minute, chosen for a combination of convenience and resolution, the electron beam spends approximately one minute on the sample area displayed on the oscilloscope, or about 0.03 seconds per sampling grid square. The X-ray count rates determine the number of frames necessary to generate enough counts per grid square so variations in X-ray intensity due to elemental concentration differences are not masked by poor counting statistics. A larger number of frames results in reduced statistical errors but causes blurring of sharp concentration edges due to electron beam drift in the EM column, especially at high magnifications. No significant blurring occurs on our EM with 25 frames or less at magnifications of 2000×.

Smoothing X-ray intensity data

Smoothing the X-ray intensities eliminates most of the variations due to statistical errors and small scale sample topography. To remove statistical and topographic variations but avoid smoothing out real variations in elemental concentration, the computer checks the eight immediate neighboring matrix points. If all the points fall within two standard deviations of the value of the central point, Gaussian smoothing is applied to the central point. If any of the surrounding points fall outside the admissible

range, a significant concentration slope is indicated and no smoothing occurs. Points on the edge of the intensity matrix are not smoothed.

Normalizing X-ray intensities

In the scanning mode, detected X-ray intensity is a function of element concentration and beam position on the sample. A normalizing procedure removes the position effect, making the X-ray intensities comparable for all points on the scanned area. During spectrometer alignment on the microanalyzer, the electron beam operates in the stationary or spot mode, locating the beam at the center of the visible rastered area. When a spectrometer is fully focused, the bombarded spot on the sample, focusing crystal and detector slit are all on the focusing circle. The plane of the focusing circle is perpendicular to the plane of the sample. The finite width of the crystal and the detector slit generate a series of focusing circles in parallel planes to give a focusing cylinder. The trace of the focusing cylinder on the sample surface is a line close to the Y deflection axis.

When the beamscanner generates an X-ray image of a homogeneous sample, the focusing cylinder-sample surface trace appears as a ridge of higher X-ray intensity. As the electron beam scans from the left to the right of the image, it passes through the focusing cylinder surface. When the electron beam hits the sample at a point on the focusing cylinder-sample surface trace, the spectrometer is in focus. As the beam moves away from the focusing trace, the focus deteriorates and the X-ray intensity measured by the spectrometer decreases. At low magnification (<500×) the X-radiation detected may become negligible when the electron beam is at the right or left edge of the image.

The radiation drop-off rate depends mostly upon the degree of perfection of the analyzing crystal used. An imperfect analyzing crystal allows greater angular divergence of reflection of a particular X-ray wavelength and can detect X-rays from a greater width of the sample than a spectrometer with a more perfect crystal. Increased imperfection of the crystal reduces the resolution of the spectrometer while increasing the thickness of the focusing cylinder wall. On our EM one mica crystal is more nearly perfect than the others. This mica crystal resolves close X-ray peaks at the expense of a rapid intensity drop-off towards the right and left edge of an image.

X-ray photon images collected from an area on a homogeneous smooth sample showed X-ray intensity variation with beam position best described by a downward opening hyperbola or parabola with the maximum value at the center of the line. At different Y positions there is little variation in the horizontal distribution curves although the maximum X-ray intensity shifts horizontally as a linear function of Y. A least squares fitted third-order surface function seemed to describe the variation in X-ray intensities over the sample surface without introducing spurious variations:

$$I_s(x,y) = a_1 + a_2x + a_3y + a_4x^2 + a_5xy + a_6y^2 + a_7x^3 + a_8x^2y + a_9xy^2 + a_{10}y^3 \quad (1)$$

where $I_s(x,y)$ is the intensity of the standard at coordinates x,y and a_i is the constant coefficient for ith term. The X-ray intensity surfaces vary in shape with the element, spectrometer and magnification, requiring a standard surface for each different combination of these variables.

Data grouping for ZAF correction

We may compute the concentration of an analyte in a sample:

$$C_A(x,y) = C_s(x,y) \cdot \frac{I_A(x,y)}{I_s(x,y)} \cdot \frac{F_s}{F_A} \quad (2)$$

where s and A refer to the standard and unknown analyte respectively, and C, I, and F are respectively the analyte or standard element concentration, X-ray intensity, and number of frames (number of scans over the image area). This first approximate concentration is adjusted for matrix effects: absorption, secondary fluorescence and atomic number effects (ZAF).

Calculation of the matrix or ZAF correction could be excessively time consuming. The application of the X-ray ZAF corrections would take up several hours if each point in the data matrix were treated separately. Results from the ZAF correction might be satisfactory when correction factors, calculated for one point, are applied to compositionally similar points.

To form compositional families, the computer groups the points according to the first concentration estimates for each element measured. A composition identifier is constructed for each of the 2000 sample points from the normalized X-ray intensity data. Each composition identifier is a 16 bit data word consisting of 8 bit-pairs. The location of the bit-pair within the data word identifies the

element while the values stored in the bit-pairs 00, 01, 10 and 11 represent the ranges 0–20, 20–50, 50–80 and 80–100% respectively of the maximum concentration measured for that element on the analyzed sample surface. Many points will have the same composition identifier suggesting similar though not necessarily identical composition. Each different composition identifier represents a unique compositional family of known average composition.

The number, and concentration ranges of the families depend on the maximum concentration value of each element in an analyzed sample. If a point on the sample indicates a 100% value for an element, that element will be split into the ranges of 0–20, 20–50, 50–80 and 80–100%. If the maximum for an element is only 60% at any point on the data map, that element will be split into the ranges 0–12, 20–30, 30–48 and 48–60%. This limiting method ensures that the four-way grouping of an element creates smaller, compositionally more accurately defined families.

It is also possible to group families assuming non-zero concentration minima for one or more elements, further improving the representation of compositional families; however, doing so complicates programming.

The ZAF correction

The absorption, secondary fluorescence, and atomic number effects (ZAF) are the matrix effects. We used for the ZAF correction a modified and abbreviated version of the ABFAN2 program (Hadidiacos *et al.*, 1971). The large size of ABFAN2, due to the extensive data matrices, made it impractical to execute on the H316 computer. Since only a small fraction of the ABFAN2 data was needed, the data matrices were replaced by a small routine that would use only the necessary information for each element. The rest of the program was streamlined.

The program generates a composite correction factor for each analyzed element in the sample for the effects of absorption (F_a), fluorescence (F_s) and atomic number (F_z). The analyte concentration at any point x,y is given by

$$C_A = R\, C_s \cdot \frac{I_A F_s}{I_s F_A} \cdot (F_a F_s F_z). \qquad (3)$$

Correction factors are determined for each compositional family once. The resulting factors are applied to all the points on the sample having the compositional identifier for that compositional family.

Elemental ratioing

In many geologic applications the absolute quantities of certain elements are not as important as the ratios of two or more elements. This ratio can often identify areas composed of a particular mineral or show zonation by emphasizing fluctuations in concentrations of alternating replacement elements within a mineral. The sum of the concentrations of two elements may also be useful.

The resulting map of ratios can be contoured by the mapping program. The general form of the ratio, R, is

$$R = k \cdot \frac{a + b}{c + d},$$

where a, b, c, and d represent elements identified by their spectrometer number and k is a scale factor. One or more of the identifiers a, b, c or d may be equivalent or left blank resulting in the following possible combinations:

$$\frac{a}{b + c}, \frac{a}{a + b}, \frac{a}{b}, \frac{a + b}{a + c}, \frac{a + b}{a} \text{ and } \frac{a + b}{c}.$$

If either numerator or denominator goes below 10 percent of its maximum value, the ratio is set to zero to avoid unpredictable ratios when counts near background give poor counting statistics. If both identifiers in the numerator or the denominator are left blank, a "1" is substituted as the value used in the calculation. This results in the additional combinations:

$$\frac{a}{1}, \frac{1}{1}, \frac{a + b}{1} \text{ and } \frac{1}{a + b}.$$

Results

In the following presentation of compositional maps, quantitative contour specifications have been removed from the maps for reproduction. Concentration highs are indicated by 'H' and lows by 'L'.

Ilmenite in magnetite—dots versus contours

Figures 5 through 7 show comparative presentations of X-ray scan data from an ore specimen. The sample comprises a cluster of ilmenite crystals in magnetite. Figures 5 and 6 show the iron distribution, while Figures 5 and 7 show the titanium concentration in the ilmenite. The variation in X-

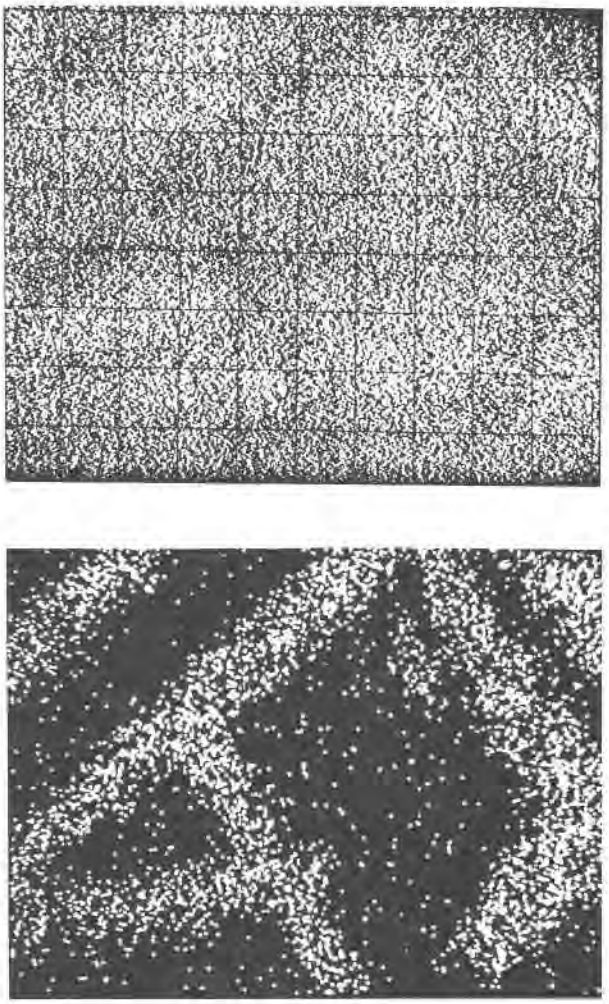

Fig. 5. Beam scanner dot photographs of iron and titanium of ilmenite crystals in magnetite. Top, iron dot pattern. Bottom, titanium dot pattern defining ilmenite crystals.

ray photon intensity from iron is barely discernible in the dot photograph of Figure 5. Figure 6 shows the very close correlation between the low iron and high titanium concentrations in Figure 7. The contours in Figure 7 occur at intervals of ten percent of the highest titanium concentration, starting at zero titanium concentration. In Figure 6 a different contouring method has been applied. Since both ilmenite and magnetite contain iron but in different amounts, the lowest iron concentration serves as a base for the contours which are spaced at ten percent intervals between the lowest and highest concentration values of any point on the map. This latter technique accentuates the difference in iron concentration between ilmenite and magnetite areas and shows small variations in iron concentration not visible using photographic techniques. Line scans across the sample confirmed continuous variation of iron and titanium from the interior to the boundary of the ilmenite crystals shown in both dot photographs and maps.

Normalizing intensity data

Figures 8, 9 and 10 illustrate normalization to correct for spectrometer defocusing. Figure 8 shows the relative intensity surface from a pure iron standard. The off-center location of the highest point on the standard surface suggests that the spectrometer used to collect the data defocused asymmetrically and was focused in such a way as to maximize the minimum count rate on the entire surface rather than maximizing the count rate of the center of the image. Figure 9 shows distribution of measured X-ray intensities from a cross-section of the inside edge of a steel tube corroded by geothermal brines. The lower, blank part of the image shows no iron within the tube. The upper part shows the X-ray intensity distribution as measured by the computer. Normalizing produces the surface shown in Figure 10 by dividing each point on Figure 9 by the corresponding point on Figure 8. On the normalized surface there is little change in iron concentration within the section of the map representing the steel tube. The lower concentration of iron in the central part of the tube in the image is real and this anomaly may have been the cause for the increased corrosion of the edge of the tube immediately below. The normalization tends to be less reliable at the right and left edges of the image due to increased statistical variation as a percentage of measured concentration.

Topographic and compositional effects on X-ray intensity contour maps

Using a more accurate numerical method to portray composition in two dimensions accentuates detrimental effects such as the focusing effect that dot photographs subdue. Two effects shown plainly with contouring are topography and atomic number effects.

Figures 11 and 12 illustrate the effect of sample topography on X-ray intensities recorded by spectrometers at opposite positions relative to the sample. The sample of Figures 11 and 12 constructed for this purpose, comprises a cross section of a steel tube containing a steel wire. Polishing caused a relatively soft silica–aluminum gel between the wire

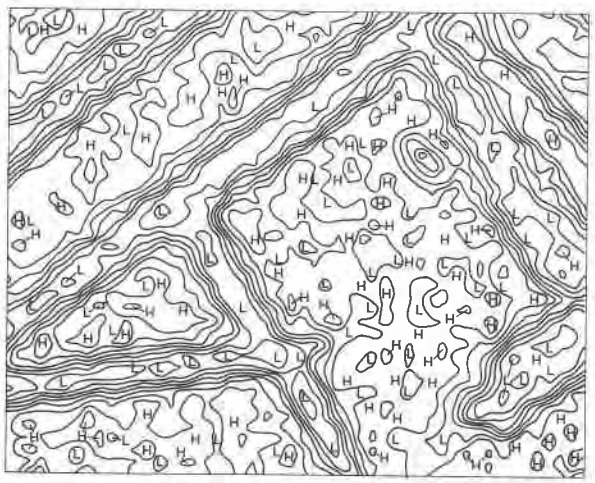

Fig. 6. Contour map of iron content of ilmenite in magnetite as in Figure 5. Low iron content in elongate ilmenite crystals and high iron content in magnetite.

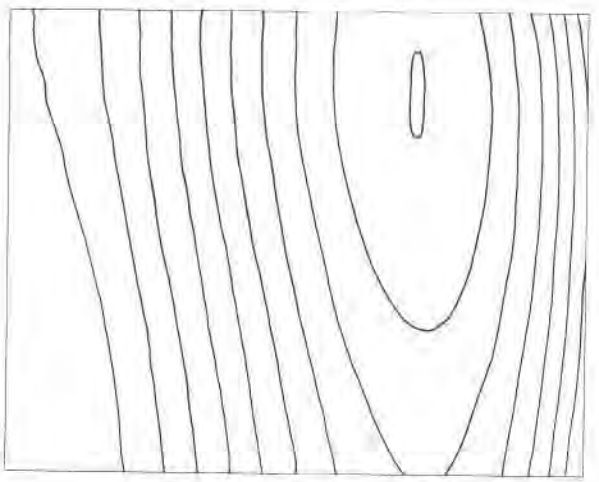

Fig. 8. X-ray intensity map of a flat surface of pure iron at 500× showing defocusing of spectrometer over the scanned sample surface.

and the tube to form a slight depression in the sample surface.

The computer-collected iron X-ray intensities, using two opposing spectrometers (goniometers), give contour maps showing high iron X-ray photon counts in the lower left (tube) and upper right (wire) corners. The contours are drawn at ten percent intervals up to the maximum count for each map.

The contours in Figures 11a and 11b differ most below 20 percent and above 80 percent of the maximum count. At low iron concentration the contours should be little affected by counting statistics. The count error is a large percentage of the mean count but a small percentage of the constant contour interval. However, comparing the maps shows that there is a significant difference between the location of the low contours. The lower contours in the lower left part of Figure 11b are farther into the gel zone than the corresponding contours in Figure 11a. Conversely, in the upper right corner the low contours in Figure 11a have moved into the gel zone relative to Figure 11b. The shifting of these low contours is due to the shadowing and fluorescence effects of the raised iron edge. As the electron

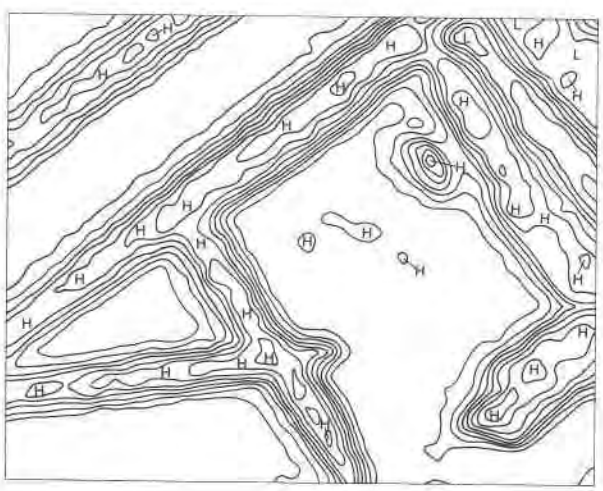

Fig. 7. Contour map of titanium content of ilmenite in magnetite as in Figure 5. High titanium content in elongate ilmenite crystals.

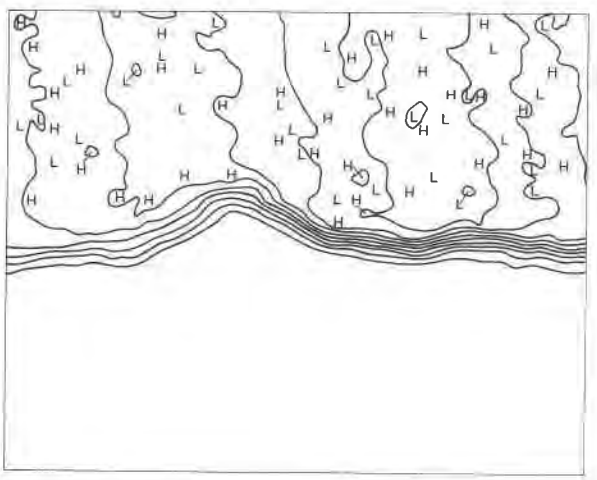

Fig. 9. Contour map of iron concentration along the cross-section of a tube wall of a geothermal steam conduit, uncorrected for spectrometer defocusing. Uniform iron concentration above interface shows apparent concentration gradient to right and left of a concentration high to the right of center. Note correspondence with gradients of Figure 8.

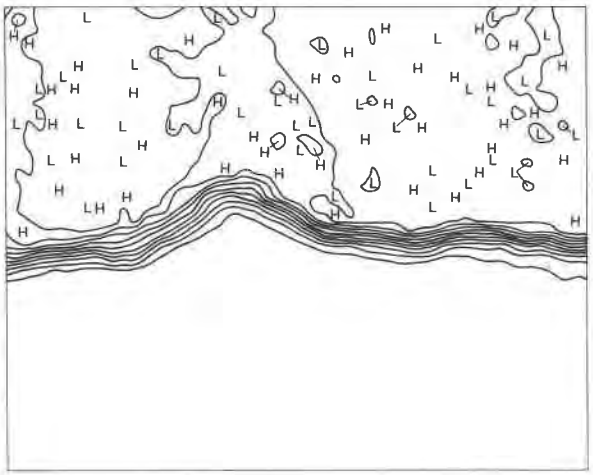

Fig. 10. Contour map of iron concentration of same area as Figure 9, corrected for defocusing. The concentration surface is nearly flat except at extreme left and at reentrant in center due to corrosion by geothermal solutions.

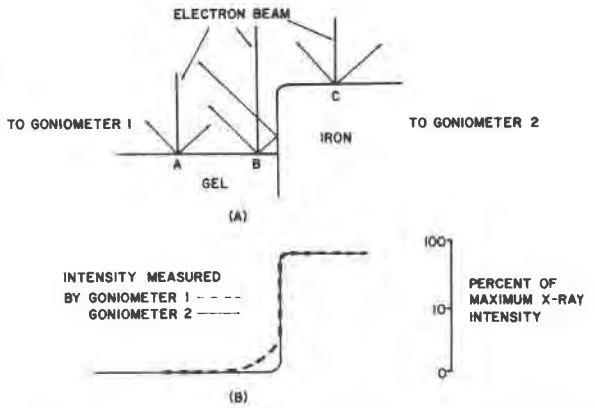

Fig. 12. Paths of electron beam and X-rays and resulting X-ray intensity for iron interface in upper right of Figures 11a and 11b. (a) Paths of electron beam and emitted X-rays relative to measuring goniometers. (b) Relative X-ray intensity measured by each goniometer.

beam scans over the sample surface, the beam-sample interaction point disappears behind the iron edge depending upon the relative position of the detecting spectrometer. Figure 12 schematically illustrates the effect for the upper right boundary in Figure 11.

An analogous effect occurs and is displayed on contour maps of topographically smooth samples near boundaries of two compositions where one composition differs from the adjoining composition greatly in absorption coefficients and fluorescent yields.

Mapping of a zoned feldspar

An example comparing an elemental contour diagram with a dot-photograph of a zoned plagioclase feldspar illustrates the advantages of the contouring method. Figure 13 shows the calcium concentration map produced using data from the same area on the crystal shown in Figures 1 and 2. This contour map is easily interpreted and shows the relationship between the calcium concentration and the light and dark zones in the crystal on the

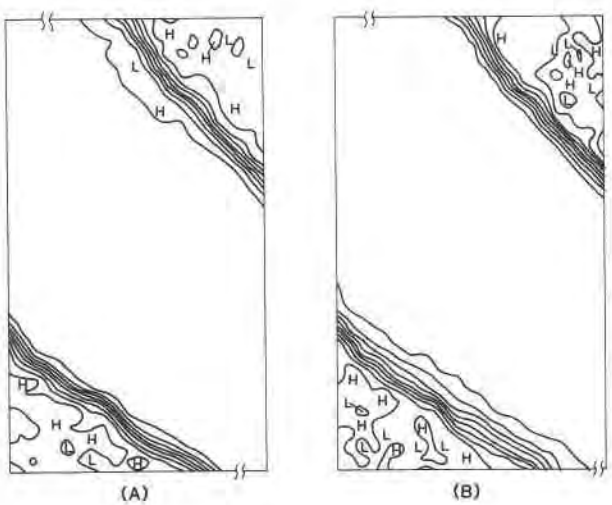

Fig. 11. Iron concentration in areas having two sharp iron interfaces as measured by two opposing spectrometers (goniometers). Iron surface is topographically higher than $Al(OH)_3$–SiO_2 gel between. (a) goniometer 1 measuring from lower left; (b) goniometer 2 measuring from upper right.

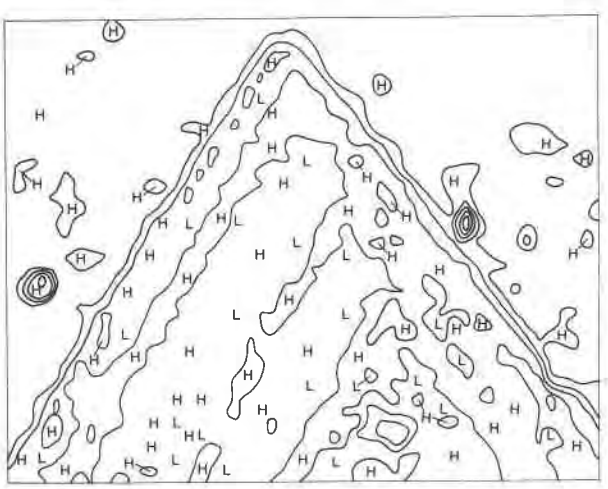

Fig. 13. Calcium concentration map of part of the zoned plagioclase crystal of Figures 1 and 2. Two high-calcium concentrations near crystal edges are calcium silicate inclusions in ground-mass crystals.

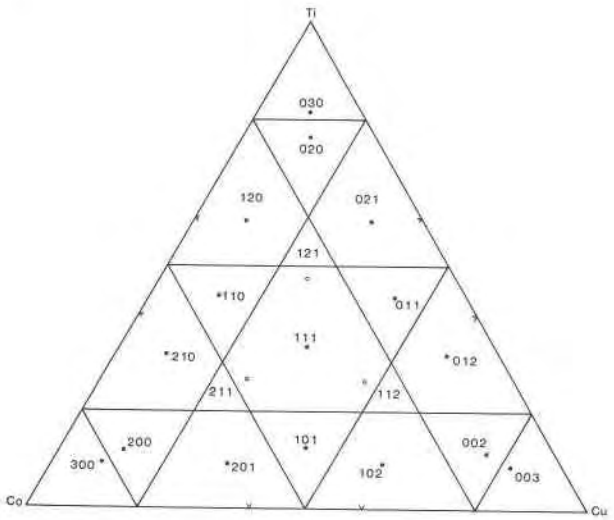

Fig. 14. Compositional families in the ternary system Ti–Co–Cu, allowing 0–100% of each component. The family is designated by a three digit number indicating the compositional range for Co, Ti and Cu respectively. The lowest composition range value is zero, the highest is three. Open circles represent compositions lying outside their families.

photograph in Figure 2. Two peaks, showing very high X-ray intensities to the right and left of the crystal on the contour map represent two small inclusions of calcium silicate. These inclusions were too small to generate enough adjacent dots on the photo in Figure 1 to allow them to be identified. The extreme proximity of the contours identifying each inclusion indicates that the source of the X-rays lies within the boundaries of only one or two sampling squares. The inclusions are really very much smaller than indicated in Figure 13 illustrating one weakness of the method.

ZAF corrections on compositional families

Before illustrating the application of ZAF correction to produce a quantitative map, we present the results of grouping X-ray data matrix corrections into compositional families.

Figure 14 shows the families occurring in a normalized three element system which exhibits absorption and fluorescence. Each element occurs in concentrations ranging up to 100% and is split at the 20, 50 and 80% concentration levels. The numbers identify 19 families and the range of the element concentrations for each family. The family 210 contains 50–80% Co, 20–50% Ti and 0–20% Cu. A dot identifies the compositional point at which the ZAF correction factors are generated for the family. The coordinates of the points are determined by normalizing the average concentration value of each element range for the family. Sometimes this method generates a point (open circle) outside the actual range of the family, *i.e.*, family 112, Figure 14, but usually it is close enough to give reasonably accurate elemental correction factors.

Figure 15 shows how the reduction of the maximum concentration affects the number, location and size of the families. The maximum concentration values for Co, Ti and Cu are 85, 70 and 80% respectively. The number of families in this ternary system has increased to 31 and each has a smaller compositional range.

We examined the maximum errors introduced by matrix correction by family for a Co–Ti–Cu alloy, and they appear to be smaller than systematic and random data collection errors. Cobalt absorbs Cu$K\alpha$ radiation resulting in enhancement of Co$K\alpha$ radiation intensity. Titanium absorbs both Co$K\alpha$ and Cu$K\alpha$ radiation but in differing fractions. Given the first approximations of the elemental concentrations the ZAF program calculates the composite correction factor for each element. When the maximum of each element in the test sample varies, the ZAF program generates the composite correction factor at a variety of points on the triangular coordinate system. Figure 16 shows the values and distribution of the composite correction factors for the element Co over the 0–100% compositional range of the elements Co, Ti and Cu.

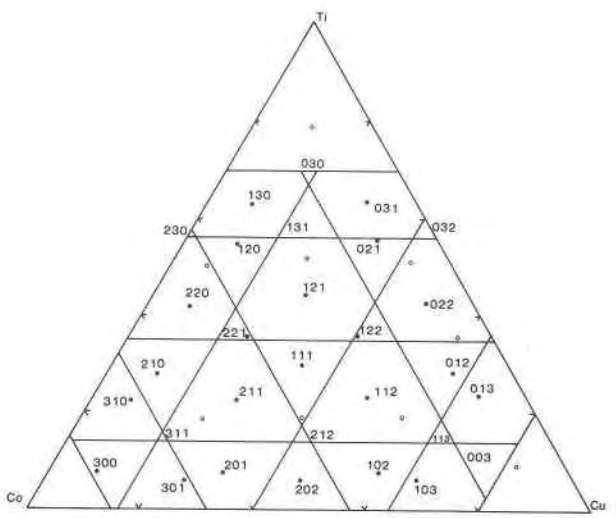

Fig. 15. Compositional families in the ternary system Ti–Co–Cu, allowing compositional ranges of 0–85, 0–70 and 0–80% for Co, Ti and Cu respectively.

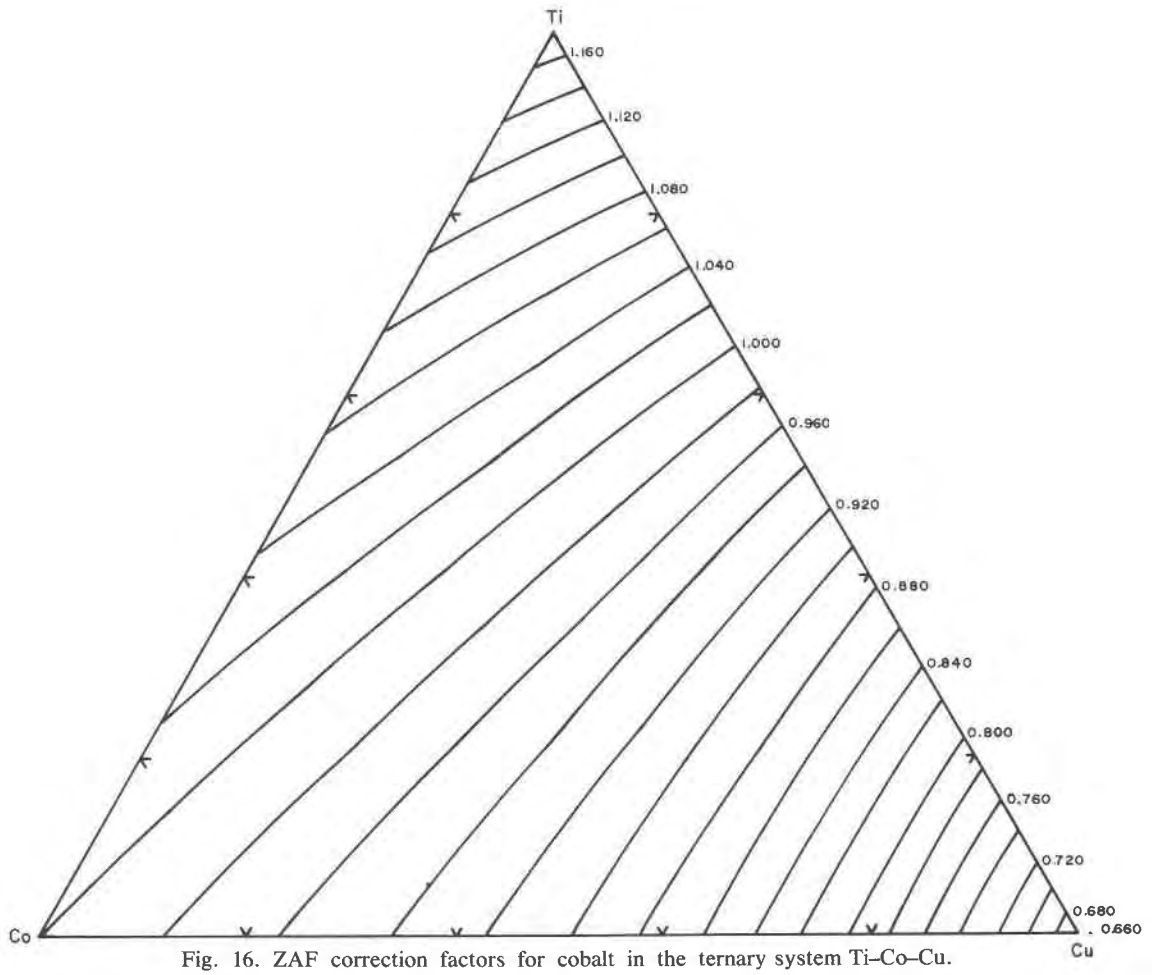

Fig. 16. ZAF correction factors for cobalt in the ternary system Ti–Co–Cu.

For an alloy containing concentrations ranging up to 100% for each element, the family ranges and factor calculation points are distributed as shown in Figure 14. Superimposing Figure 14 on each of the elemental correction factor diagrams, the range of factors within each family, and the factor applied to that element in that family, can be determined. The deviation of the factor applied at a point from the "correct" factor at that point determines the error in the resulting concentration value. Table 1 lists the maximum error in the correction factor within each family represented in Figure 14.

The errors in Table 1 show that the factor errors for Ti and Cu are within acceptable limits for EM analysis. Several of the errors for the cobalt correction factor appear unacceptable. However, the cobalt concentration at the points producing the greatest errors is near zero so that the error in the overall sample analysis is not significant. The error in the cobalt correction factor decreases rapidly for points that contain more significant quantities of cobalt. Although the correction factors for the families identified as 121, 211 and 112 are calculated at a point outside the area covered by the family, the maximum factor errors are not only within but at the low end of the range of errors for the other families.

In most samples, 100% concentrations of each of the analyzed elements are unlikely within a small sample area. Depending upon the sample investigated, the maximum distributions as indicated for Figure 15, 85% Co, 70% Ti and 80% Cu may be more realistic. When Figure 15 is superimposed on Figures 16 and 17, the maximum errors obtained for the families are significantly smaller than the results from Table 2. In most families the average error in the factor applied to the elemental concentration is less than half the listed maximum error.

Table 1. Maximum errors in correction factors for compositional families in Ti–Co–Cu system. Each element occurs in maximum concentrations of 100 percent.

FAMILY	MAXIMUM ERROR, % Ti	Co	Cu
002	2.1	8.8	2.4
003	2.0	17.0	2.8
011	0.5	4.2	2.0
012	0.9	12.0	2.5
020	0.8	5.1	2.4
021	1.1	6.6	2.8
030	2.3	6.4	3.1
101	1.5	5.3	2.1
102	1.8	7.9	2.9
110	0.8	3.1	2.0
111	1.4	5.8	2.7
112	0.9	4.6	1.2
120	1.4	6.0	2.2
121	0.3	3.5	0.9
200	1.2	2.2	2.4
201	2.5	4.7	3.0
210	1.3	4.0	2.7
211	0.7	1.6	1.8
300	2.1	2.3	2.0
Mean Error	1.35	5.85	2.31

Table 2. Maximum errors in correction factors for compositional families in Ti–Co–Cu system. The maximum concentration of each element is Ti–70%, Co–85%, Cu–80%.

FAMILY	MAXIMUM ERRORS, % Ti	Co	Cu
003	1.5	7.7	1.9
012	0.7	5.4	1.5
013	1.0	7.0	1.8
021	0.3	3.4	1.2
022	0.3	6.8	2.0
023	0.0	2.9	1.1
030	0.8	3.9	1.0
031	0.4	4.4	2.0
032	0.4	1.7	1.7
102	1.5	4.9	1.9
111	0.8	2.9	1.4
112	1.3	6.0	2.1
113	0.7	5.6	1.1
120	o.5	3.3	1.3
121	0.8	4.3	2.0
122	0.4	2.4	1.2
130	0.8	2.9	1.6
131	0.5	4.0	1.0
201	1.4	3.0	2.0
202	1.7	4.0	1.6
210	0.8	2.2	1.7
211	1.7	4.0	2.2
212	0.5	1.3	0.5
220	0.8	3.4	1.8
221	0.4	1.6	0.9
230	0.1	2.2	0.8
300	1.2	1.9	1.7
301	1.7	2.3	1.9
310	1.1	2.3	1.8
311	0.8	0.9	1.4
Mean Error	0.85	3.75	1.55

Quantitative analysis

To illustrate quantitative analysis we synthesized a control specimen of known composition which would give appreciable ZAF corrections. The specimen was Stainless Steel 308 welded by Inconel 82. We then analyzed the weld boundary area where the steel had dissolved into the inconel and the inconel had diffused a short distance into the steel. Significant compositional values are as follows: inconel—72.0% Ni, 3.0% Fe, 20.0% Cr.; stainless steel—10.0% Ni, 67.0% Fe, 20.7% Cr. Figure 17 shows the map of nickel concentration at the boundary of the weld. Correct percentages of nickel at the extreme top and extreme bottom of the map are 37. and 10. respectively. The equivalent percentages ignoring the ZAF correction are 34. and 8.5 respectively.

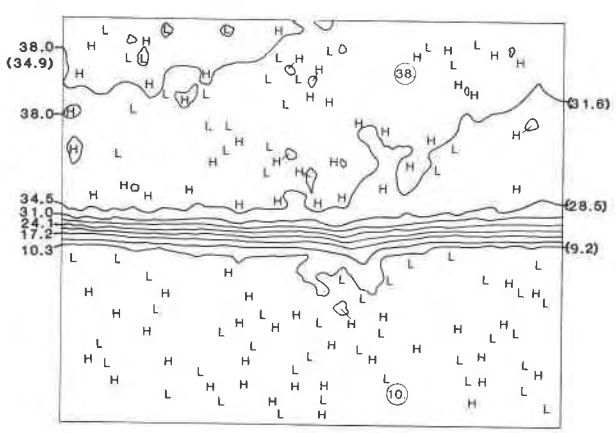

Fig. 17. Quantitative analysis of Ni at weld boundary between Inconel 82 (top) and Steel 308 (bottom). Steel dissolved in inconel. Contour numbers represent weight percent. Numbers in parentheses are weight percent without ZAF correction. Circled numbers are "true" weight percent.

Discussion

Compositional mapping works well and works with minimum modification to an EM. All but the data collection programs can be written in FORTRAN. The method is easily applicable to old EM's but is most suited to the newer EM's. Our laboratory now uses compositional mapping for about 50% of our EM work.

For new EM's with integral computers, no hardware modifications are necessary to do compositional mapping. At least one of the new EM's has analyzing crystals that have a rocking motion coor-

dinated with beam sweep, helping to eliminate defocusing over the image area, simplifying programming and allowing mapping at lower magnifications.

Although compositional mapping provides a new way for the study of minerals, it has some disadvantages. We have compared mapping with point counting along lines across zones of artificial plagioclase crystals. The point counts along the line showed very well the stepwise decrease in calcium outward from the grain center. However, compositional mapping showed zones badly obscured by calcium highs caused by tiny inclusions of calcium silicate. The coarseness of the 50 × 40 grids accentuated the effect of the inclusions. If, as on the newer EM's, X-ray intensities could have been collected from only the center of each grid square through digital control of the beam, then only an occasional inclusion would be in the beam.

Very sharp compositional boundaries of mineral grains where an element concentration changes from a very high value to or near zero "smears" to give a width to the region where none exists. The smearing results from several factors: (1) finite beam diameter; (2) contouring method; (3) sampling of all of each sampling grid square, instead of one point of the grid square; (4) smoothing; (5) topography at boundaries; (6) real smearing of the boundaries during sample polishing and (7) random statistical errors in the X-ray intensities. Sampling only one point per grid square coupled with smoothing could improve the boundary definition significantly. Currently, when looking critically at a boundary area, we simply increase the magnification from 500× to 1000× or 2000× which almost doubles or quadruples boundary resolution.

Finally, compositional mapping can work on EM's or scanning electron microscopes equipped with energy dispersive systems. Using energy dispersive detectors eliminates the spectrometer defocusing corrections, but complicates and increases data collection timing.

References

Birks, L. S. (1971) Electron Probe Microanalysis, ed. 2, Wiley-Interscience, New York.

Cullity, B. D. (1956) Elements of X-Ray Diffraction, Addison-Wesley, Reading, Massachusetts.

Hadidiacos, G. G., Finger, L. W., and Boyd, F. R., (1971) Computer reduction of electron probe data. Carnegie Institution Year Book, 69, (1969–1970), 294.

Hall, C. E. (1966) Introduction to Electron Microscopy, ed. 2, McGraw-Hill, New York.

Heinrich, K. F. J. (1964) Instrumental developments for electron microprobe readout. Advances in X-Ray Analysis, 7, 382.

Hitchings, J. R. (1976) Color aids data interpretation. Research/Development, 27, 26.

Ingersoll, R. M., and Derouin, D. H. (1969) Application of color photography to electron microbeam probe samples. Review of Scientific Instruments, 40, 637.

Tomura, T., Okano, H., Hara, K. and Watanabe, T. (1968) Multistep intensity indication in scanning microanalysis. Advances in X-Ray Analysis, 11, 316.

Manuscript received, April 2, 1980;
accepted for publication, January 19, 1982.